JACS
JOURNAL OF THE AMERICAN CHEMICAL SOCIETY

ARTICLE

pubs.acs.org/JACS

Bypass of Aflatoxin B$_1$ Adducts by the *Sulfolobus solfataricus* DNA Polymerase IV

Surajit Banerjee,[§] Kyle L. Brown, Martin Egli, and Michael P. Stone*

Departments of Chemistry and Biochemistry, Center in Molecular Toxicology, Vanderbilt Institute of Chemical Biology, and the Vanderbilt-Ingram Cancer Center, Vanderbilt University, Nashville, Tennessee 37235, United States

S *Supporting Information*

ABSTRACT: Aflatoxin B$_1$ (AFB$_1$) is oxidized to an epoxide in vivo, which forms an N7-dG DNA adduct (AFB$_1$−N7-dG). The AFB$_1$−N7-dG can rearrange to a formamidopyrimidine (AFB$_1$−FAPY) derivative. Both AFB$_1$−N7-dG and the β-anomer of the AFB$_1$−FAPY adduct yield G→T transversions in *Escherichia coli*, but the latter is more mutagenic. We show that the *Sulfolobus solfataricus* P2 DNA polymerase IV (Dpo4) bypasses AFB$_1$−N7-dG in an error-free manner but conducts error-prone replication past the AFB$_1$−FAPY adduct, including misinsertion of dATP, consistent with the G→T mutations observed in *E. coli*. Three ternary (Dpo4−DNA−dNTP) structures with AFB$_1$−N7-dG adducted template:primers have been solved. These demonstrate insertion of dCTP opposite the AFB$_1$−N7-dG adduct, and correct vs incorrect insertion of dATP vs dTTP opposite the 5′-template neighbor dT from a primed AFB$_1$−N7-dG:dC pair. The insertion of dTTP reveals hydrogen bonding between the template N3 imino proton and the O^2 oxygen of dTTP, and between the template T O^4 oxygen and the N3 imino proton of dTTP, perhaps explaining why this polymerase does not efficiently catalyze phosphodiester bond formation from this mispair. The AFB$_1$−N7-dG maintains the 5′-intercalation of the AFB$_1$ moiety observed in DNA. The bond between N7-dG and C8 of the AFB$_1$ moiety remains in plane with the alkylated guanine, creating a 16° inclination of the AFB$_1$ moiety with respect to the guanine. A binary (Dpo4−DNA) structure with an AFB$_1$−FAPY adducted template:primer also maintains 5′-intercalation of the AFB$_1$ moiety. The β-deoxyribose anomer is observed. Rotation about the FAPY C5−N^5 bond orients the bond between N^5 and C8 of the AFB$_1$ moiety out of plane in the 5′-direction, with respect to the FAPY base. The formamide group extends in the 3′-direction. This improves stacking of the AFB$_1$ moiety above the 5′-face of the FAPY base, as compared to the AFB$_1$−N7-dG adduct. Ternary structures with AFB$_1$−β-FAPY adducted template:primers show correct vs incorrect insertion of dATP vs dTTP opposite the 5′-template neighbor dT from a primed AFB$_1$−β-FAPY:dC pair. For dATP, the oxygen atom of the FAPY formamide group participates in a water-mediated hydrogen bond with Arg332. The insertion of dTTP yields a structure similar to that observed for the AFB$_1$−N7-dG adduct. The differential accommodation of these AFB$_1$ adducts within the active site may, in part, modulate lesion bypass.

■ INTRODUCTION

Aflatoxins are metabolites of *Aspergillus flavus* and related fungi that contaminate food crops.[1−4] Aflatoxin B$_1$ (AFB$_1$; Chart 1A) is mutagenic in bacteria,[2,5−7] tumorogenic in fish,[8,9] carcinogenic in rodents[10,11] and is implicated in the etiology of human liver cancer.[4,12,13] Aflatoxin exposures are implicated in mutations to the p53 tumor suppressor gene.[14−20] The metabolism of AFB$_1$ involves oxidation to AFB$_1$-*exo*-8,9-epoxide by cytochromes P450.[21−25]

AFB$_1$-*exo*-8,9-epoxide reacts with DNA to yield the AFB$_1$−N7-dG adduct *trans*-8,9-dihydro-8-(N7-guanyl)-9-hydroxyaflatoxin B$_1$ (Chart 2A).[2,26] This is attributed to intercalation of the epoxide above the 5′-face of deoxyguanosine in DNA,[27] facilitating the nucleophilic attack by the N7 nitrogen at the C8 carbon of the epoxide.[28] The AFB$_1$−N7-dG adduct undergoes base-catalyzed hydrolysis of the imidazole ring to form the AFB$_1$ formamidopyrimidine adduct (AFB$_1$−FAPY) (Chart 2A).[29] The AFB$_1$−FAPY adduct interconverts between α and β anomers of the deoxyribose moiety (Chart 2B).[30] In duplex DNA the AFB$_1$−β-FAPY anomer is favored, but in single strand DNA, a 2:1 α:β equilibrium mixture of anomers is observed.[30] Additionally, the AFB$_1$−FAPY adduct can undergo conformational rearrangements involving atropisomers about the C5-N^5

bond and geometrical isomers of the formyl moiety.[30] Note the change in numbering in going from the AFB$_1$−N7-dG adduct to the AFB$_1$−FAPY adduct; the C5−N^5 bond in the AFB$_1$−FAPY adduct corresponds to the C5−N7 bond in the AFB$_1$−N7-dG adduct.

The genotoxicity of AFB$_1$ has been ascribed to the AFB$_1$−β-FAPY adduct, which induces high levels of G→T transversions[31] associated with AFB$_1$ mutagenesis in *Escherichia coli*,[6] whereas the cationic AFB$_1$−N7-dG adduct is less mutagenic.[32] Moreover, the AFB$_1$−β-FAPY adduct is persistent in vivo.[33−35] Smela et al.[31] demonstrated that an oligodeoxynucleotide containing an AFB$_1$−FAPY adduct equilibrated between two separable species, one of which was mutagenic whereas the other blocked DNA replication. These correspond to the α and β anomers of the AFB$_1$−FAPY adduct: the mutagenic species is the AFB$_1$−β-FAPY adduct; the AFB$_1$−α-FAPY adduct blocks replication.[30]

In DNA the AFB$_1$−β-FAPY adduct intercalates with the AFB$_1$ moiety on the 5′-face of the pyrimidine moiety of the adducted nucleotide,[36,37] similar to the initially formed AFB$_1$−N7-dG adduct.[38−41] The stability of the AFB$_1$−β-FAPY adduct in
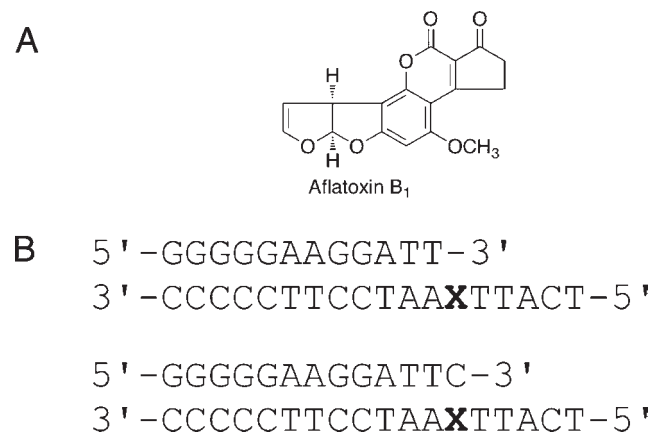
DNA is attributed to robust interstrand stacking interactions.[36,37] The AFB$_1$–α-FAPY adduct also intercalates above the 5′-face of the damaged base.[42] The lower stability of the AFB$_1$–α-FAPY as compared to the AFB$_1$–β-FAPY adduct[36,37] is attributed to structural perturbations in the DNA and reduced interstrand stacking interactions.[42] The similar 5′-intercalation of the AFB$_1$–N7-dG[38−41] and AFB$_1$–β-FAPY[36] adducts are consistent with each producing G→T transversions in *E. coli*, but do not readily explain the increased mutagenicity of the AFB$_1$–β-FAPY adduct.[31]

To understand why the AFB$_1$–β-FAPY adduct is more mutagenic than is the AFB$_1$–N7-dG adduct,[31] we have utilized the *Sulfolobus solfataricus* P2 DNA polymerase IV (Dpo4) polymerase as a model system by which to examine the bypass of the AFB$_1$–N7-dG[38−41] and AFB$_1$–β-FAPY[36] adducts. We find that this Y-family polymerase bypasses the AFB$_1$–N7-dG adduct in an error-free manner but bypasses the AFB$_1$–β-FAPY adduct much less efficiently and in an error-prone fashion. Three ternary (Dpo4–DNA–dNTP) structures with AFB$_1$–N7-dG adducted template:primers provide structural insight into the bypass of these lesions. These reveal correct insertion of dCTP at the AFB$_1$–N7-dG damage site and correct insertion of dATP vs incorrect insertion of dTTP opposite the 5′-template neighbor dT from a primed AFB$_1$–N7-dG:dC base pair (Chart 1B). The insertion of dTTP involves hydrogen bonding between the template N3 imino proton and the O^2 oxygen of dTTP, and between the template T O^4 oxygen and the N3 imino proton of dTTP, perhaps explaining why this polymerase does not efficiently catalyze phosphodiester bond formation from this mispair. The AFB$_1$ moiety intercalates above the 5′-face of the alkylated guanine.[38−41] The bond between N7-dG and C8 of the AFB$_1$ moiety remains in plane with the alkylated guanine, creating a 16° inclination of the AFB$_1$ moiety with respect to the alkylated guanine. A binary (Dpo4–DNA) structure with a AFB$_1$–FAPY adducted template:primer reveals the β-deoxyribose anomer at the polymerase active site. The C5–N^5 bond is in the R_a axial conformation, as observed for the AFB$_1$–β-FAPY adduct,[36,37] and the nucleoside and the FAPY base,[30] which is attributed to stacking preferences of the AFB$_1$ moiety. Opening of the guanine imidazole ring allows for rotation about the C5–N^5 bond. The bond between the formamide N^5 nitrogen and C8 of the AFB$_1$ moiety shifts out-of-plane with respect to the FAPY base and orients in the 5′-direction. The formamide orients in the 3′-direction. This improves stacking of the AFB$_1$ moiety above the 5′-face of the FAPY base. Ternary structures with AFB$_1$–β-FAPY adducted template:primers reveal correct vs incorrect insertion of dATP vs dTTP opposite the 5′-template neighbor dT from a primed AFB$_1$–β-FAPY:dC base pair. For dATP, the FAPY formamide oxygen participates in a water-mediated hydrogen bond with Arg332. Overall, the differential

Chart 1. A. Structure of AFB$_1$. B. Sequences Used for Gel Extension Assays and Crystallography (X denotes either the AFB$_1$–N7-dG or AFB$_1$–β-FAPY adducts)

Aflatoxin B$_1$

B
5′-GGGGGAAGGATT-3′
3′-CCCCCTTCCTAA**X**TTACT-5′

5′-GGGGGAAGGATTC-3′
3′-CCCCCTTCCTAA**X**TTACT-5′

Chart 2. A. Formation of the AFB$_1$–FAPY Adduct via Base-Catalyzed Ring-Opening of the AFB$_1$–N7-dG Adduct. B. The AFB$_1$–FAPY Adduct Interconverts between α and β Anomers: The Equilibrium Is Dependent on Single Strand vs Duplex DNA Environments[32]
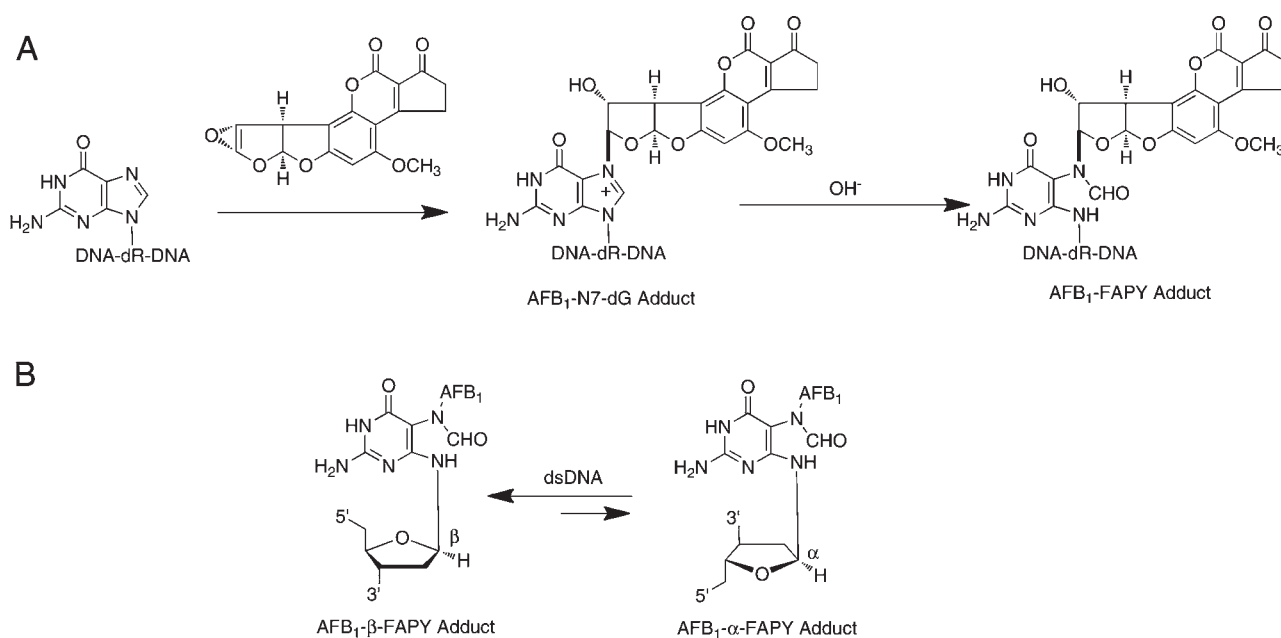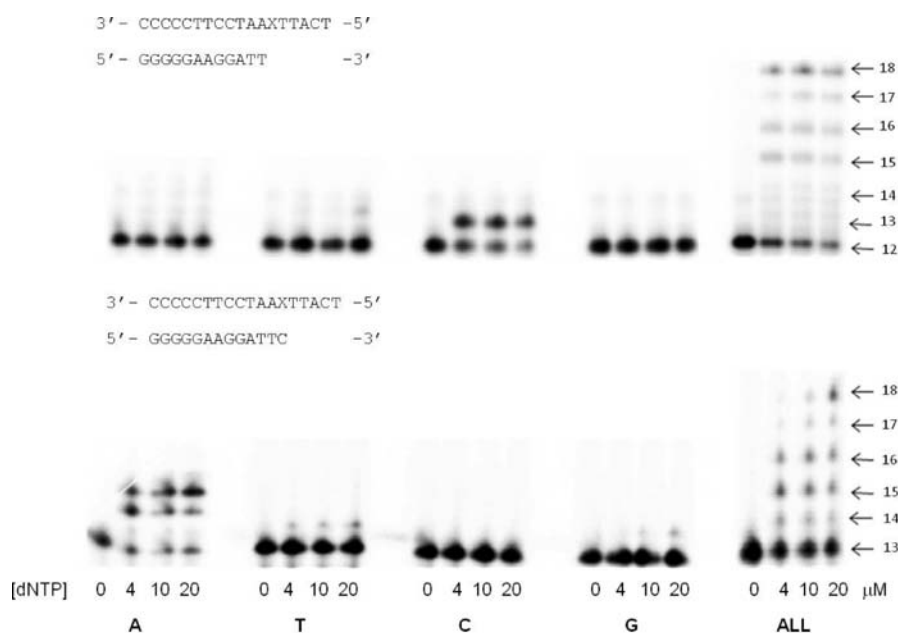
Figure 1. Replication bypass of the AFB_1-N7-dG-modified Sequence I and Sequence II template:primers with *S. solfataricus* P2 DNA polymerase Dpo4. The sequences I and II are displayed with the gels. The concentrations of the dNTPs are provided below the gels. The designations A, T, C, G represent single nucleotide insertion experiments; the designation ALL represents the full-length extension assay incorporating all four dNTPs. Each assay was incubated for 1 h at 37 °C.

accommodation of these AFB_1 adducts within the active site may play a role in modulating lesion bypass by this polymerase.

■ RESULTS

Synthesis of Site-Specifically AFB_1-N7-dG- and $AFB_1-\beta$-FAPY-Modified Templates. The oligodeoxynucleotide 5′-d-(TCATTGAATCCTTCCCCC)-3′, containing the targeted N7-dG alkylation site (underlined), was annealed with 5′-d-(ATTCAAT)-3′ to form a partially double-stranded scaffold. This was reacted with AFB_1 *exo*-8,9-epoxide in a biphasic mixture. The product 5′-d(TCATTXAATCCTTCCCCC)-3′ (X = AFB_1-N7-dG) was separated from unreacted 5′-d-(TCATTGAATCCTTCCCCC)-3′ and 5′-d(ATTCAAT)-3′ using HPLC. The AFB-N7-dG-modified oligodeoxynucleotide was characterized by mass spectrometry. The pH was then shifted to pH 10 at 37 °C, to form a mixture of $AFB_1-\alpha$-FAPY and $AFB_1-\beta$-FAPY lesions that were separated by HPLC and characterized by mass spectrometry.

Single Nucleotide Insertion Assays. *a. AFB_1-N7-dG Adduct.* Figure 1 (top panel) shows the results of single nucleotide insertion assays using the Sequence I 18mer:12mer template:primer (Chart 1B). The concentrations of dNTPs used in the experiments were 4, 10, and 20 μM. The Dpo4 polymerase exhibited a strong preference for the correct insertion of dCTP opposite the AFB_1-N7-dG lesion. When all four dNTPs were included in the reaction, the polymerase extended the primer to the full-length 18-mer product. Figure 1 (bottom panel) shows the results of single nucleotide insertion assays using the Sequence II 18mer:13mer template:primer (Chart 1B). This experiment monitored single nucleotide extension beyond the correctly inserted dC at the 3′-terminus of the primer. Again, the concentrations of dNTPs used in the experiments were 4, 10, and 20 μM. The polymerase correctly inserted dATP twice, corresponding to the positioning of the two thymines 5′ to the

AFB_1-N7-dG lesion in the template. When all four dNTPs were included in the reaction, the polymerase extended the primer to the full-length 18-mer product.

b. $AFB_1-\beta$-FAPY Adduct. Figure 2 (top panel) shows the results of single nucleotide insertion assays using the Sequence I 18mer:12mer template:primer. The Dpo4 polymerase was less efficient at inserting nucleotides opposite the $AFB_1-\beta$-FAPY lesion. Consequently, in these experiments the concentrations used for dNTPs were increased to 15, 30, and 60 μM. Under these conditions, the correct nucleotide dCTP was inserted opposite the $AFB_1-\beta$-FAPY lesion but low levels of the incorrect nucleotide dATP were also inserted. In the dATP lanes, weak bands were observed corresponding to the 14-mer and 15-mer products, suggesting that multiple insertions of dATP occurred, presumably involving the two 5′-neighboring template dT nucleotides in the template strand, perhaps coupled with strand slippage. Thus, the $AFB_1-\beta$-FAPY lesion showed both correct insertion of dCTP and error-prone insertion of dATP for this template:primer. When all four dNTPs were included in the reaction, at concentrations of 50, 100, and 250 μM, the polymerase successfully extended the primer to the full-length 18-mer product. Figure 2 (bottom panel) shows the results of single nucleotide insertion assays using the Sequence II 18mer:13mer template:primer. This experiment monitored single nucleotide extension beyond the correctly inserted dC at the 3′-terminus of the primer. The polymerase was less efficient at extending nucleotides past the $AFB_1-\beta$-FAPY adduct, as compared to the AFB_1-N7-dG adduct. Consequently, in these experiments the concentrations used for dNTPs were increased to 15, 30, and 60 μM. The polymerase did not efficiently insert any dNTP in the single nucleotide extension reaction, although again in the dATP lanes, weak bands were observed, which probably correspond to multiple insertions of dATP opposite the 5′-neighboring dT nucleotides in the template. When all four dNTPs were
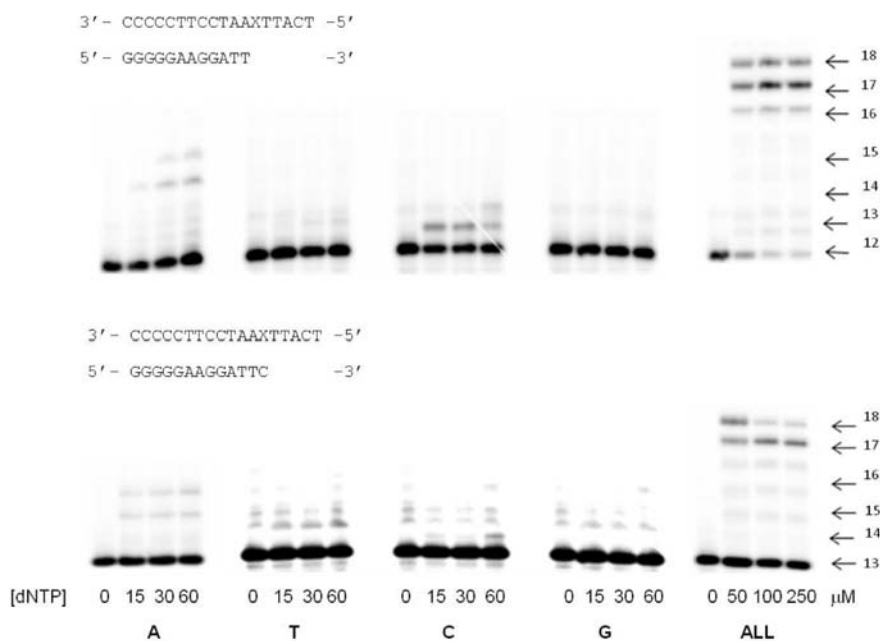
Figure 2. Replication bypass of the $AFB_1-\beta$-FAPY-modified Sequence I and Sequence II template:primers with *S. solfataricus* P2 DNA polymerase Dpo4. The sequences I and II are displayed with the gels. The concentrations of the dNTPs are provided below the gels. The designations A, T, C, G represent single nucleotide insertion experiments; the designation ALL represents the full-length extension assay incorporating all four dNTPs. Each assay was incubated for 1 h at 37 °C.

included in the reaction, at concentrations of 50, 100, and 250 μM, the polymerase extended the primer to the full-length 18-mer product.

Crystallization, Data Collection, and Data Processing. When the AFB_1-N7-dG-modified template was annealed with Sequence I, the 12-mer primer, the resulting template:primer was primed for insertion of dNTP opposite the template AFB_1-N7-dG adduct (Chart 1B). When the AFB_1-N7-dG-modified template was annealed with Sequence II, the 13-mer primer, the resulting template:primer was primed for insertion of dNTP opposite the template 5′-neighbor T (Chart 1B). Likewise, when the $AFB_1-\beta$-FAPY-modified template was annealed with Sequence I, the resulting template:primer was primed for insertion of dNTP opposite the template AFB_1-N7-dG adduct. When the $AFB_1-\beta$-FAPY-modified template was annealed with Sequence II, the resulting template:primer was primed for insertion of dNTP opposite the template 5′-neighbor T. Using the Sequence I 12-mer primed for insertion of dNTP opposite the AFB_1-N7-dG adduct, a ternary complex with incoming dCTP was crystallized and X-ray diffraction data were collected. Using the Sequence II 13-mer primer, with a dC complementary to either the AFB_1-N7-dG or $AFB_1-\beta$-FAPY adducts, ternary complexes with incoming dATP or dTTP were crystallized and X-ray diffraction data were collected.

With Sequence I, the complex containing the AFB_1-N7-dG adduct exhibited the lowest symmetry crystal system with the *P*1 space group. The crystals exhibited needle shape morphologies. They exhibited fragility under the synchrotron source. Due to the triclinic crystal system, the completeness was lower as compared to the other data sets. To increase the completeness, multiple data sets were scaled together. For the ternary complex with the Sequence I 12-mer primer, the structure was solved with incoming dCTP in the triclinic crystal system at 2.9 Å resolution. The unit cell showed half of the volume compared to the

orthorhombic crystal systems for the other complexes, by making the *a*-axis approximately half of the usual size. The Matthew coefficient favored two molecules in the asymmetric unit. Using a reported Dpo4–DNA complex[43] as a search model, CNS[44] and MOLREP[45,46] gave two solutions with close correlation coefficients. The dimer of the asymmetric unit was selected by viewing the different solution in the unit cell. As both of the molecules are unique in the solution, it was found that one was more ordered because it was more covered by electron density. The DNA extending out of the active site was more disordered in one molecule than the other. To avoid model bias, the incoming dCTP was placed opposite to the guanine moiety of the AFB_1-N7-dG adduct, using difference Fourier analysis. When complexed with the Sequence II 13-mer primer, the 18-mer template containing the AFB_1-N7-dG adduct crystallized in $P2_12_12$ space group. The structures were solved with incoming dATP or dTTP, in the orthorhombic system with 2.8 and 3.0 Å resolutions, respectively. The statistics of data processing and data quality for the ternary AFB_1-N7-dG complexes are summarized in Table S1 in the Supporting Information.
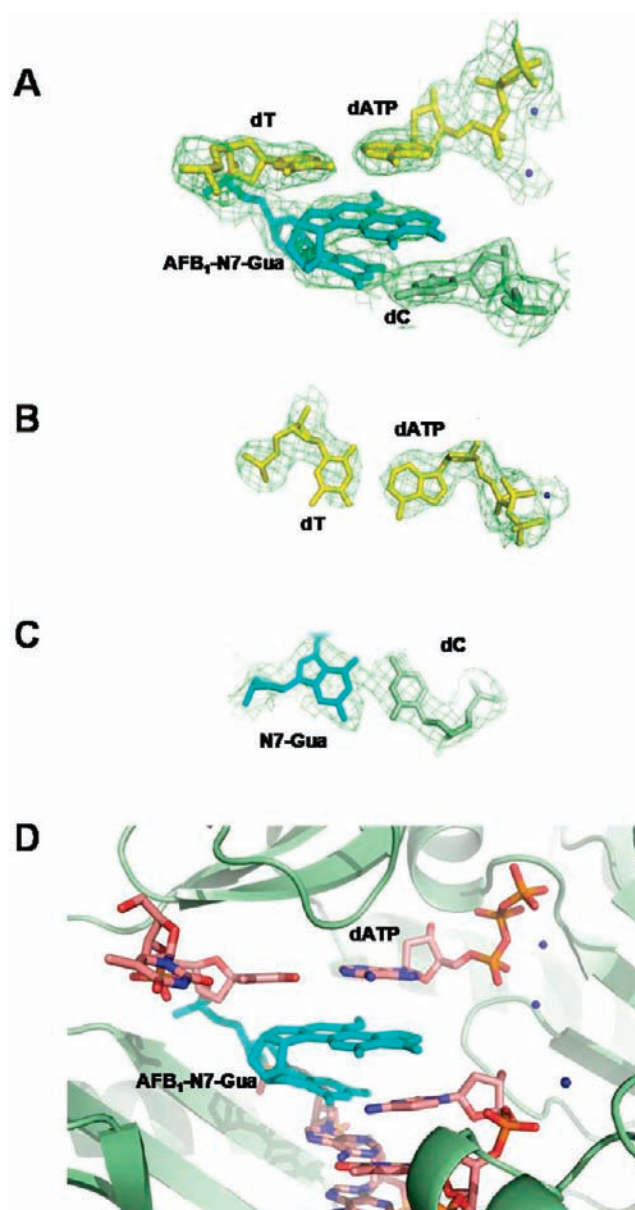
The Dpo4 polymerase was cocrystallized with the $AFB_1-\beta$-FAPY-modified template and the Sequence II 13-mer primer in the absence of dNTP (binary complex), and the structure was determined at 3.0 Å resolution. For the $AFB_1-\beta$-FAPY adduct each of the ternary complexes with the Sequence II 13-mer primer, one with incoming dATP and the other with incoming dTTP, crystallized in orthorhombic systems. The data were complete with a good amount of redundancy. Matthew coefficients were calculated to measure the solvent content for each of the crystals. The structures of the ternary complexes were determined at 2.9 and 2.7 Å resolutions for the dATP and dTTP complexes, respectively. The statistics of data processing and data quality for the $AFB_1-\beta$-FAPY adduct are summarized in Table S2 in the Supporting Information.
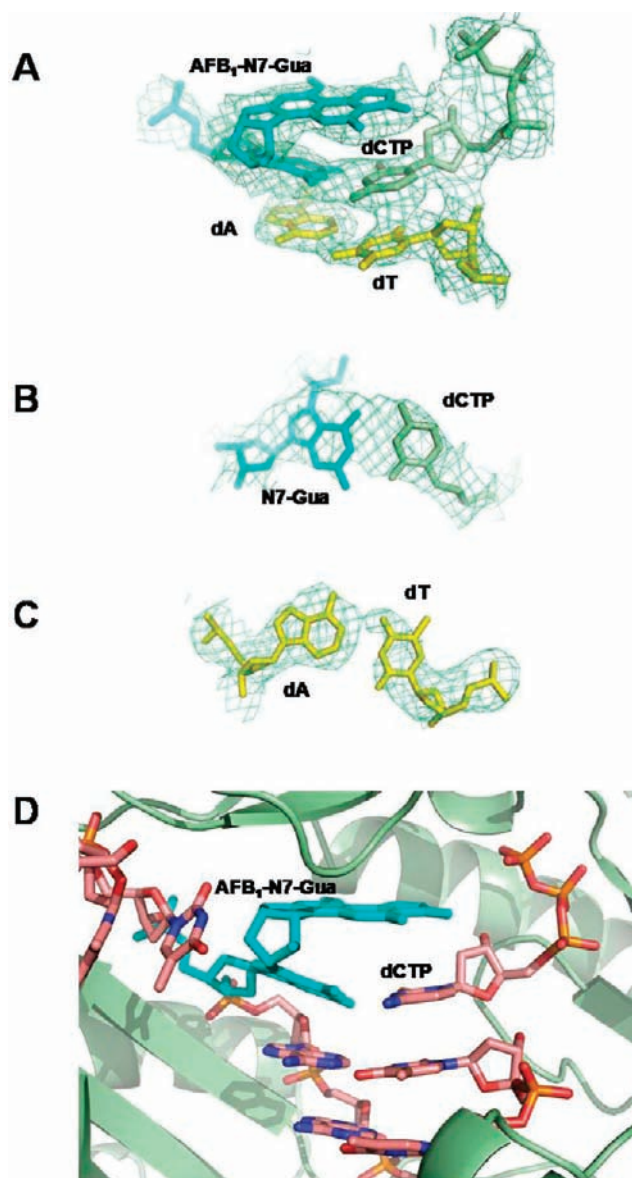
Figure 3. Structure of the ternary AFB$_1$−N7-dG-modified Sequence I template:primer complex with the *S. solfataricus* P2 DNA polymerase Dpo4 and incoming dCTP. A. Electron density at the active site. B. Watson−Crick base pair between AFB$_1$−N7-dG and 3′-primer terminus dC. C. Watson−Crick dA:dT base pair involving the template 3′-neighbor dA. D. Active site with the modified template:primer and the dCTP along with the polymerase. The Dpo4 is colored green and the AFB$_1$−N7-dG adduct is colored cyan. All electron densities are from $(2F_o − F_c)$ maps at the 1σ level.
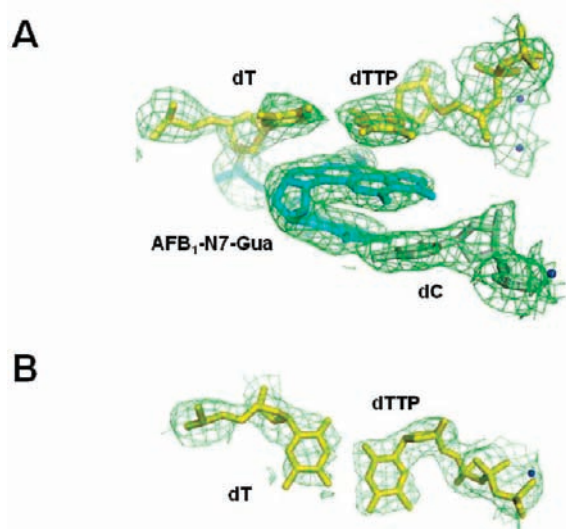
Figure 4. Structure of the ternary AFB$_1$−N7-dG-modified Sequence II template:primer complex with the *S. solfataricus* P2 DNA polymerase Dpo4 and incoming dATP. A. Electron density at the active site. B. Watson−Crick base pair between the 5′-template neighbor T and incoming dATP. C. Watson−Crick base pair between AFB$_1$−N7-dG and 3′-primer terminus dC. D. Active site with the modified template: primer and the dATP along with the polymerase. The Dpo4 is colored green and the AFB$_1$−N7-dG is colored cyan. The Ca^{2+} ions are shown as blue spheres. All electron densities are from $(2F_o − F_c)$ maps at the 1σ level.

Ternary Complex Showing Correct Insertion of dCTP Complementary to the AFB$_1$−N7-dG Adduct. The electron density at the polymerase active site placed the AFB$_1$ moiety intercalated above the 5′-face of the adducted guanine base (Figure 3). The AFB$_1$ methoxy group faced toward the minor groove of the template strand, while the keto oxygens of the AFB$_1$ moiety faced into the nascent duplex. The guanine and AFB$_1$ moieties at the adduct site were 16° out of plane with respect to each other. This was a consequence of the sp^2 hybridization at the N7 atom, which placed the bond between N7-dG and C8 of AFB$_1$ in plane with the alkylated guanine,

consistent with the electron density. The incoming dCTP was opposite to the guanine base of the AFB$_1$−N7-dG adduct. It wedged between the AFB$_1$ moiety and the damaged guanine base. The potential for Watson−Crick hydrogen bonding between the incoming dCTP and the guanine base of the AFB$_1$−N7-dG adduct remained intact (Figure 3B). On the 3′-side of the adduct, the dA (template):dT(primer terminus) base pair remained inserted into the duplex but was slightly sheared. In one monomer unit, the Ca^{2+} site near to the primer terminus
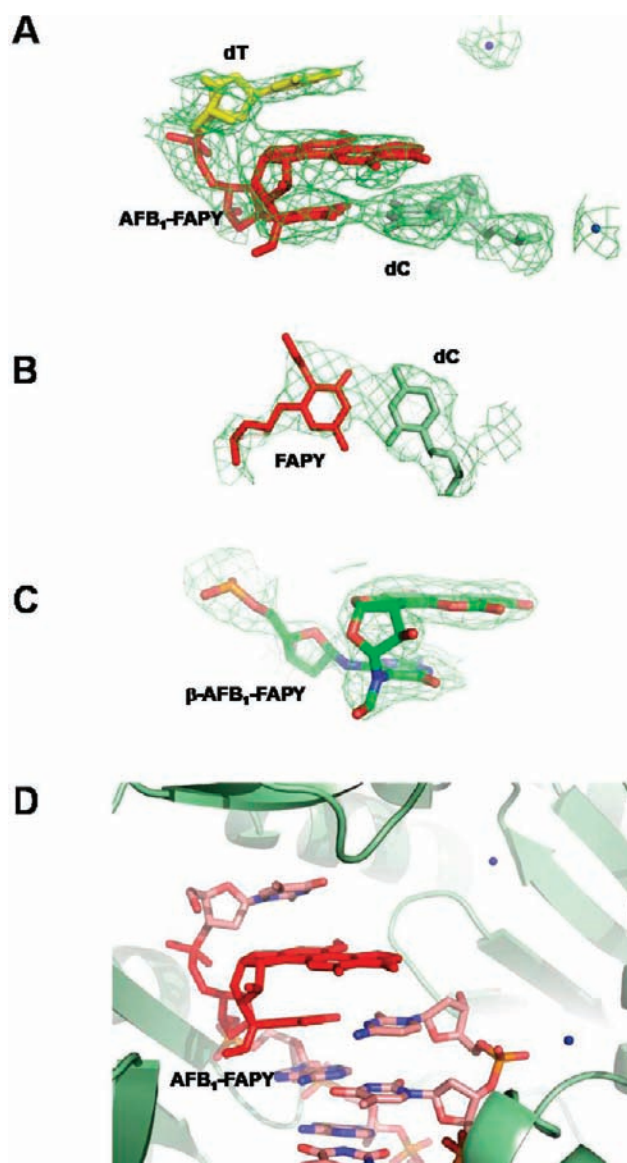
Figure 5. Structure of the ternary AFB$_1$—N7-dG-modified Sequence II template:primer complex with the *S. solfataricus* P2 DNA polymerase Dpo4 and incoming dTTP. A. Electron density at the active site. B. Hydrogen bonding between the 5′-template neighbor T and incoming dTTP. All electron densities are from $(2F_o - F_c)$ maps at the 1σ level.

Figure 6. Structure of the binary AFB$_1$—β-FAPY-modified Sequence II template:primer complex with the *S. solfataricus* P2 DNA polymerase Dpo4. A. Electron density at the active site. B. Watson—Crick base pair between the FAPY base of the AFB$_1$—β-FAPY adduct and 3′-primer terminus dC. C. The electron density of the AFB$_1$—β-FAPY nucleoside. D. Active site with the modified template:primer along with the polymerase. The Dpo4 is colored green and the AFB$_1$—N7-dG is colored cyan. The Ca^{2+} ions are shown as blue spheres. All electron densities are from $(2F_o - F_c)$ maps at the 1σ level.

was found, which was missing in the other monomeric unit. A similar observation was made for the Ca^{2+} site near the triphosphate of dCTP. This lower symmetry structure showed two monomers in the asymmetric unit with unique features. The distance between the 3′-hydroxyl group of the primer to the α-phosphate of incoming dCTP varied from 3.1 to 5.2 Å for the two molecules. For both molecules, the active site Ca^{2+} ions were not found but were refined with water oxygens, assuming disordered sites for them.

Ternary Complex Showing Correct Insertion of dATP from the AFB$_1$—N7-dG:dC Primer. Figure 4A shows the electron density map at the polymerase active site, with the correct incoming dATP placed opposite to the template 5′-neighbor dT. The incoming dATP stacked above the AFB$_1$ moiety and was positioned to form Watson—Crick hydrogen bonds with the template dT (Figure 4B). Watson—Crick base pairing was maintained between the guanine base of the AFB$_1$—N7-dG adduct and the primer 3′-terminus dC (Figure 4C). However, at the adduct site, both the guanine base and dC of the primer tilted out of plane toward the 3′-direction of the template. The AFB$_1$ moiety remained intercalated above the 5′-face of the modified guanine base. The distance between the α-phosphate of the incoming dATP and the 3′-OH group of the primer was 6.7 Å. The Ca^{2+} ion near to the primer terminus was within 4 Å of the oxygen atoms of phosphate group between the 12th and 13th primer nucleotides.

Ternary Complex Showing Misinsertion of dTTP from the AFB$_1$—N7-dG:dC Primer. Figure 5A shows the electron density map at the polymerase active site, with the incorrect dTTP placed opposite to the template 5′-neighbor dT. The overall structure of the polymerase with the dNTP binding site was similar to that observed for the ternary complex showing correct insertion of dATP, described above. The AFB$_1$ moiety intercalated between the damaged guanine base and template 5′-T. The primer 3′-terminus dC maintained Watson—Crick hydrogen bonding with the damaged guanine base. The damaged base and primer 3′-terminus dC tilted in the 3′ direction with respect to the

template. The distance between the alpha phosphate and the primer 3′-OH group was 6.0 Å. The Ca^{2+} ion near to the primer 3′-terminus was within 4 Å of the oxygen atoms of phosphate between the 12th and 13th primer nucleotides. Figure 5B shows the electron density of the incorrect dTTP placed opposite to the template 5′-neighbor dT. It was positioned to form hydrogen bonds between the N3 imino proton of the template T and the O^2 keto oxygen of the incoming dTTP, and between the O^4 keto oxygen of the template T and the N3 imino proton of the incoming dTTP. This pairing arrangement shifted the incoming dTTP toward the minor groove, relative to the position it would assume in a nascent A:T base pair.
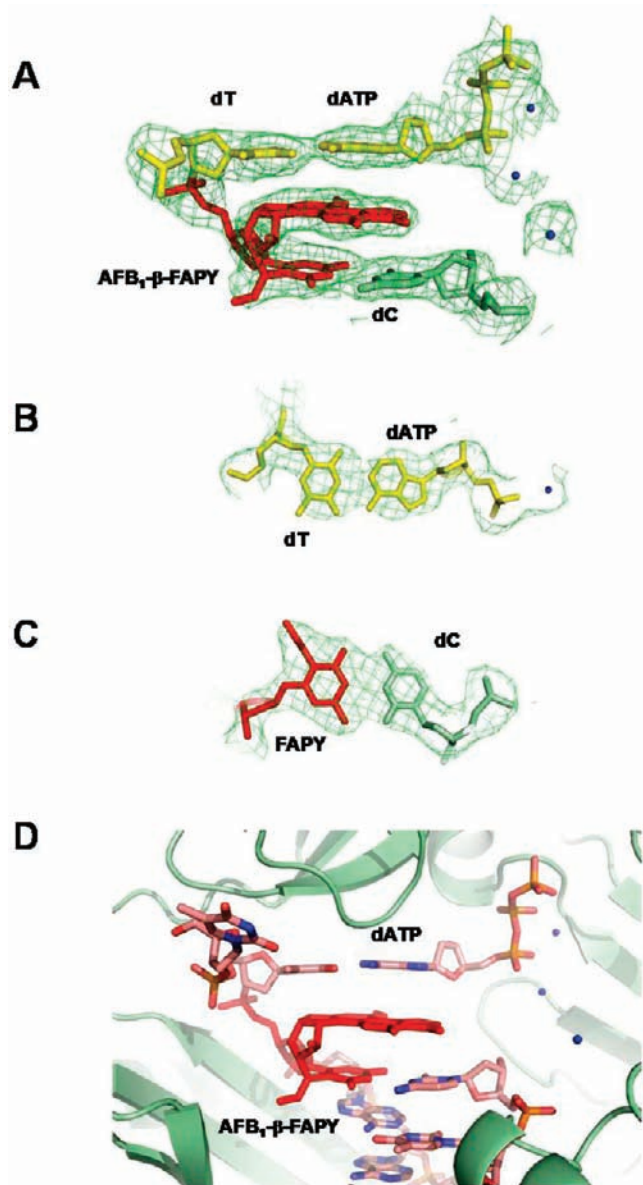
Figure 7. Structure of the ternary $AFB_1-\beta$-FAPY-modified Sequence II template:primer complex with the *S. solfataricus* P2 DNA polymerase Dpo4 and incoming dATP. A. Electron density at the active site. B. Watson—Crick base pair between the 5'-template T and the incoming dATP. C. Watson—Crick base pair between the FAPY base of the $AFB_1-\beta$-FAPY adduct and 3'-primer terminus dC. D. Active site with the modified template:primer along with the polymerase and the dATP. The Dpo4 is colored green, and the $AFB_1-\beta$-FAPY is colored cyan. The Ca^{2+} ions are shown as blue spheres. All electron densities are from $(2F_o - F_c)$ maps at the 1σ level.
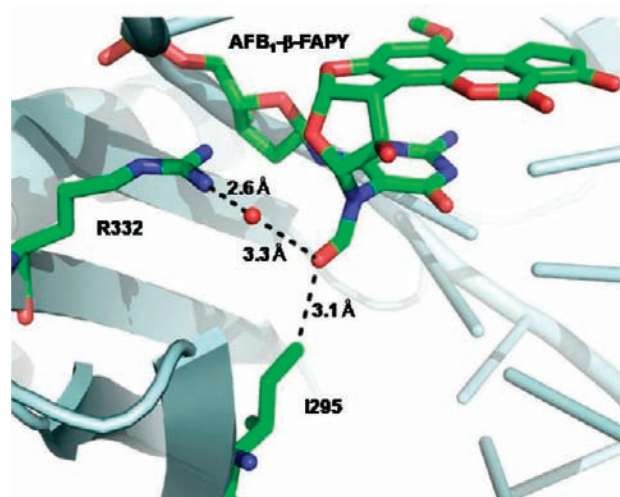

Figure 8. The water-mediated hydrogen bond network for the ternary complex with $AFB_1-\beta$-FAPY-modified Sequence II template:primer complex with the *S. solfataricus* P2 DNA polymerase Dpo4 and incoming dATP. The red sphere represents the oxygen atom of a water molecule. The distances are measured between the donor and acceptor atom.

Binary Complex with the $AFB_1-\beta$-FAPY Adduct. Figure 6 shows the electron density for the binary complex formed between the template containing the AFB_1-FAPY adduct and Sequence II, the 13-mer primer. The electron density revealed that at the lesion site the AFB_1 moiety was intercalated above the 5'-face of the FAPY base. Similar to the AFB_1-N7-dG lesion, this placed the AFB_1 methoxy group facing the minor groove of the template, with the two keto oxygens of the AFB_1 facing the major groove of the template. The deoxyribose was in the β-anomeric

configuration. The $C5-N^5$ bond was in the R_a axial conformation, as observed in DNA in solution for the $AFB_1-\beta$-FAPY adduct,[36,37] and the nucleoside and the FAPY base.[30] For the $AFB_1-\beta$-FAPY adduct hindered rotation may occur about the $C5-N^5$ bond, and this oriented the bond between the N^5 nitrogen and the C8 of AFB_1 out of plane with respect to the FAPY base and in the 5'-direction in the major groove. The formamide moiety extended toward the 3'-direction of the template, with the oxygen atom facing into the major groove. It was not positioned to hydrogen bond with the N^6 exocyclic amino group of the 3'-template neighbor dA. This differed from the AFB_1-N7-dG lesion, in which sp^2 hybridization at the N7 nitrogen required that the bond between the formamide nitrogen and the C8 atom of AFB_1 remain in plane with the base. The 5'-terminus of the template was disordered and three bases on that side from the adduct region exhibited larger thermal parameters and were discarded. The 3'-terminal dC of the primer was complementary to the FAPY base. It was positioned to form Watson—Crick hydrogen bonds with the FAPY base (Figure 6B).

Ternary Complex Showing Correct Insertion of dATP from the $AFB_1-\beta$-FAPY:dC Primer. For this complex involving the Sequence II primer, the AFB_1 moiety was parallel with the DNA base pairs and stacked between the FAPY base and 5'-neighbor dT (Figure 7A). The deoxyribose moiety was in the β-anomeric configuration. The helicoidal rise between the AFB_1 moiety and the FAPY base was approximately 3.7 Å. The incoming dATP paired with the 5'-neighbor template base dT, with conservation of Watson—Crick hydrogen bonding (Figure 7B). At the 3'-terminus of the primer, Watson—Crick hydrogen bonding was maintained between the FAPY base and the primer dC (Figure 7C). This resulted in a gap of 6.9 Å between the 3'-hydroxyl of the primer dC and the α-phosphate of the dATP (Figure 7D). The oxygen atom of the formamide group participated in a water-mediated hydrogen bond with Arg332 and made van der Waals contacts with Ile 295 (Figure 8). Three bound Ca^{2+} ions were identified (Figure 7A). The first two were in the active site for catalysis and dNTP coordination. The
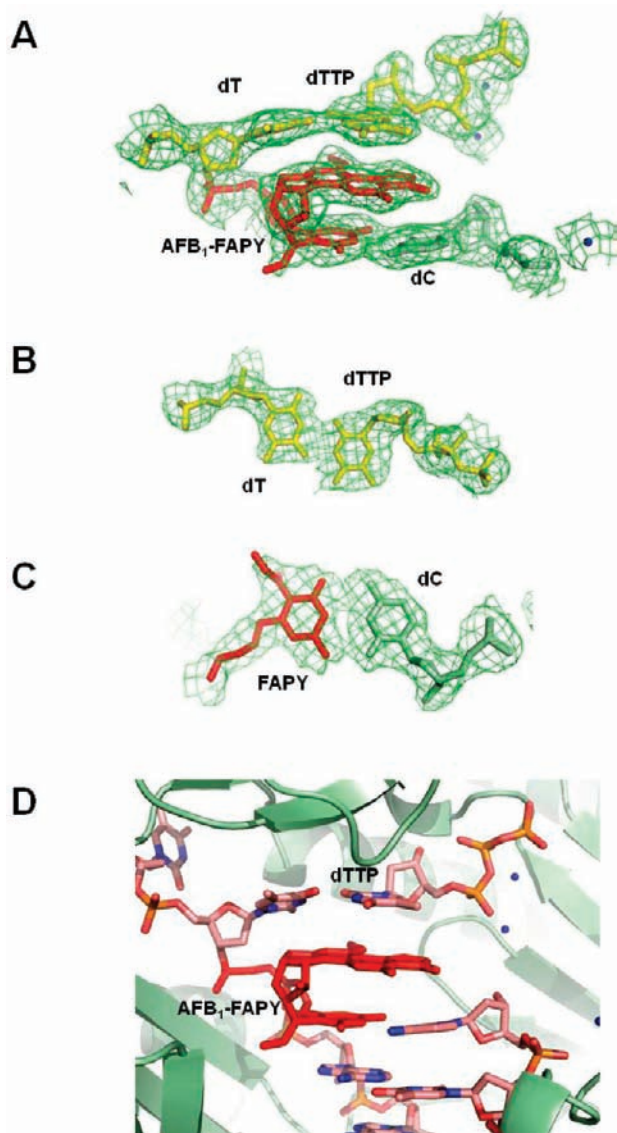
Figure 9. Structure of the ternary $AFB_1-\beta$-FAPY-modified Sequence II template:primer complex with the *S. solfataricus* P2 DNA polymerase Dpo4 and incoming dTTP. A. Electron density at the active site. B. Hydrogen bonding between the 5′-template T and the incoming dTTP. C. Watson–Crick base pair between the FAPY base of the $AFB_1-\beta$-FAPY adduct and 3′-primer terminus dC. D. Active site with the modified template:primer along with the polymerase and the dTTP. The Dpo4 is colored green, and the AFB_1-N7-dG is colored cyan. The Ca^{2+} ions are shown as blue spheres. All electron densities are from $(2F_o - F_c)$ maps at the 1σ level.

third Ca^{2+} ion was 3.0 Å from the main-chain carbonyl oxygen of Ala181 in the thumb domain of the polymerase. One Ca^{2+} ion at the active site was 3.5 Å distant from the primer 3′-terminus hydroxyl, suggesting that it was positioned to catalyze the reaction.

Ternary Complex Showing Misinsertion of dTTP from the $AFB_1-\beta$-FAPY:dC Primer. For this complex involving the Sequence II primer, the AFB_1 moiety was parallel with the DNA base pairs and stacked between the FAPY base and template 5′-neighbor dT (Figure 9A). The deoxyribose moiety was in the β-anomeric configuration. The helicoidal rise between

the AFB_1 moiety and the FAPY base was approximately 3.7 Å. The incoming dTTP was positioned complementary to the 5′-neighbor template base dT (Figure 9B). It was positioned to form hydrogen bonds between the N3 imino proton of the template T and the O^2 keto oxygen of the incoming dTTP, and between the O^4 keto oxygen of the template T and the N3 imino proton of the incoming dTTP (Figure 9B). This pairing arrangement shifted the incoming dTTP toward the minor groove, relative to the position it would assume in a nascent dA:dT base pair. At the 3′-terminus of the primer, Watson–Crick hydrogen bonding was maintained between the FAPY base and the primer dC (Figure 9C). This resulted in a gap of 6.3 Å between the 3′-hydroxyl of the primer dC and the α-phosphate of the dTTP, respectively. (Figure 9D). Three bound Ca^{2+} ions were identified (Figure 9D). The first two were in the active site for catalysis and dNTP coordination. The third Ca^{2+} ion was 3.0 Å from the main-chain carbonyl oxygen of Ala181 in the thumb domain of the polymerase. One Ca^{2+} ion at the active site was 4.9 Å distant from the primer end hydroxyl atom for the ternary complex with dTTP, suggesting that it was positioned to catalyze the reaction.

■ DISCUSSION

AFB_1 is implicated in the etiology of human liver cancer,[4,12,13] and exposures are implicated in mutations to the p53 tumor suppressor gene.[14−20] In contrast to replicative DNA polymerases, the active sites of Y-family polymerases are more solvent accessible and often can accommodate two template bases.[47−52] Moreover, the nascent base pairs may be less constrained than for replicative polymerases. These features result in a relaxed geometric selection for incoming dNTPs.[49] Finally, the stepwise conformational transitions accompanying nucleoside triphosphate binding and the nucleotidyl transfer reaction during a full replication cycle may be distinct from the translocation events in replicative polymerases.[53] Collectively, these changes compromise the efficiency and fidelity of replication. The lesion bypass ability, accuracy, and efficiency of Y-family polymerases vary[54−58] and depend on the type of DNA lesion.[59−69] Complexes with template:primers and incoming dNTPs involving the *S. solfataricus* Dpo4 polymerase, a DinB homologue,[47,48,53,57,70] have been used to model the lesion bypass efficiency and fidelity with other Y-family polymerases.[47]

Bypass of the AFB_1-N7-dG and $AFB_1-\beta$-FAPY Adducts. The Dpo4 polymerase recapitulates several aspects of the site-specific mutagenesis data observed for AFB_1 in *E. coli*.[31,32] For example, predominantly error-free bypass is observed for the AFB_1-N7-dG adduct (Figure 1), which correlates with the lower mutagenicity of this adduct observed in the *E. coli* studies.[32] The polymerase both inserts the correct dCTP opposite the damaged base and, in the presence of all four dNTPs, extends the primer to a full-length product. In contrast, with the $AFB_1-\beta$-FAPY adduct, replication bypass in vitro is less efficient and is error-prone, which correlates with the greater mutagenicity of the AFB_1-FAPY lesion in the *E. coli* studies (Figure 2).[31] Also, the Dpo4 polymerase misincorporates dATP, albeit inefficiently, when challenged by the $AFB_1-\beta$-FAPY adduct. This is anticipated to lead to a G→T transversion, in agreement with the site-specific mutagenesis studies in *E. coli*.[31] However, the Dpo4 polymerase also misincorporates other dNTPs, again inefficiently, when challenged by the $AFB_1-\beta$-FAPY adduct (Figure 2). While the Dpo4 polymerase does provide a model

system for the replication bypass of the AFB_1—N7-dG and AFB_1—β-FAPY adducts, to fully understand the G→T transversions observed in *E. coli*, it will ultimately be necessary to crystallize complexes of these adducts with the relevant polymerases in *E. coli*.

Error-Free Bypass of the AFB_1—N7-dG Adduct. The ternary complex of the AFB_1—N7-dG adduct with the Sequence I 12-mer primer, showing correct insertion of dCTP opposite the adducted guanine, is remarkable (Figure 3). It provides the first glimpse of the AFB_1—N7-dG adduct during replication bypass. The intercalation of the AFB_1 moiety above the 5′-face of the adducted guanine base, with the AFB_1 methoxy group facing toward the minor groove of the template, while the two keto oxygens of the AFB_1 moiety face into the nascent duplex, is similar to that observed in DNA.[38−41] This indicates that the damaged nucleotide is accommodated within the active site of the polymerase without significant changes to the conformation of the AFB_1 adduct in DNA. The electron density demonstrates that the adducted guanine base and AFB_1 moiety are 16° out of plane with respect to each other. This is a consequence of maintaining the bond between N7-dG and the C8 carbon of the AFB_1 moiety in plane with the damaged guanine base and had been inferred from NMR data.[40,41] While this allows for a stable stacking interaction of the AFB_1 moiety above the 5′-face of the adducted guanine base, it also creates a wedge in the DNA. During replication bypass, this perhaps facilitates the insertion of the incoming dCTP between the AFB_1 moiety and the adducted guanine base. The potential for Watson—Crick hydrogen bonding between the incoming dCTP and the guanine base of the AFB_1—N7-dG adduct remains intact (Figure 3B). The distance between the 3′-OH group of the primer to the α-phosphate suggests an active complex. This may account for the ability of the polymerase to correctly insert dCTP opposite the AFB_1—N7-dG lesion (Figure 1), consistent with the low mutagenicity of this lesion in *E. coli*.[2,32] This complex packed differently in the crystal than did the other complexes examined in this study, which may be attributed to the differential structure of the intercalated AFB_1 moiety at the active site. The structure shows greater distortion in the DNA. Consequently, the neighboring base pairs also are perturbed and the DNA backbone rearranges to conserve Watson—Crick hydrogen bonding.

The AFB_1—β-FAPY Adduct in the Polymerase Active Site. The AFB_1—FAPY lesion interconverts between α and β deoxyribose anomers; the β-anomer is preferred in duplex DNA.[30] The structure of the AFB_1—FAPY adduct in the binary complex with the Sequence I 12-mer primer indicates that at the active site the deoxyribose maintains the β-configuration (Figure 6C). The electron density indicates that the C5—N^5 bond of the pyrimidinyl moiety is in the R_a configuration as observed for the AFB_1—β-FAPY adduct,[36,37] and the nucleoside and the FAPY base.[30] Rotation about this bond allows the bond between the alkylated N^5 formamido nitrogen and the C8 of the AFB_1 moiety to orient out of plane with respect to the FAPY base and toward the 5′-direction, as was inferred from NMR.[36,37,42] This allows the AFB_1 moiety to stack efficiently with the FAPY base. The 3′-primer terminus dC forms a Watson—Crick bonding interaction with the FAPY base. In the 5′-d(TX̲A)-3′ sequence it was proposed that the downfield NMR chemical shift of the 3′-neighbor N^6-dA amino proton reflected the presence of a hydrogen bond between the N^6-dA exocyclic amino group of the 3′-neighbor adenine and the formamide carbonyl.[36,37,42] However, this is not observed in the crystal. Unlike the binary

Dpo4 complex involving native DNA,[71] in which the primer terminus reached to the extreme end of the active site, here the active site is occupied by the AFB_1—β-FAPY adduct and the template 5′-neighbor dT (Figure 6). This is attributed to the intercalation of the AFB_1 moiety above the 5′-face of the FAPY base and the stacking of the AFB_1 moiety with the template 5′-neighbor dT. The distance between the primer terminus AFB_1—FAPY:dC pair and AFB_1 is approximately 3.7 Å, which is similar to the helicoidal rise in B-DNA. In the binary complex, the conformations of the protein side chains for Y10, Y48, and R51 remain similar to those reported for the binary Dpo4 complex involving native DNA.[71]

Inefficient Bypass of the AFB_1—β-FAPY Adduct. The single nucleotide insertion assays using the Sequence I template:primer (Figure 2) indicate that the Dpo4 polymerase does not efficiently insert dNTPs opposite to the AFB_1—β-FAPY adduct. For the AFB_1—β-FAPY adduct, the parallel stacking of the AFB_1 moiety with the FAPY base may hinder access to the incoming dNTP within the active site (Figure 6). In contrast, for the AFB_1—N7-dG adduct, the adducted guanine base and AFB_1 moieties are 16° out of plane with respect to each other. The resulting wedge between the adducted guanine base and the AFB_1 moiety might allow greater access for the incoming dCTP (Figure 3), consistent with the error-free bypass of the AFB_1—N7-dG lesion (Figure 1). Thus, conformational differences of the AFB_1 moiety within the active site of the polymerase, which result from the differing orientations of the N7—C8 bond of the AFB_1—N7-dG vs the N^5—C8 bond of the AFB_1—β-FAPY adduct may, in part, modulate AFB_1 lesion bypass by this polymerase.

Implications for AFB_1-Induced Mutagenesis. The genotoxicity of AFB_1 has been ascribed primarily to the AFB_1—β-FAPY adduct,[30] which is strongly mutagenic and induces the G→T transversions[31] associated with AFB_1 mutagenesis in *E. coli*,[6] whereas the cationic AFB_1—N7-dG adduct also induces G→T transversions but is less mutagenic.[32] The present replication bypass and structural data are derived from a model system and thus cannot reveal how AFB_1 induces G→T mutations during error-prone bypass in *E. coli*. However, the Dpo4 polymerase extension data suggest that with the sequence I template:primer the correct nucleotide dCTP may be inserted opposite the AFB_1—β-FAPY lesion, but the incorrect nucleotide dATP, which would lead to a G→T transversion, may also be incorporated (Figure 2). The correct insertion of dATP opposite the template 5′-neighbor dT could lead to a G→T mutation if, following dATP insertion, strand slippage of the newly formed primer 3′-terminus dA occurs, allowing for a second insertion of dATP opposite the template 5′-neighbor dT. If strand slippage does not occur, but rather the insertion of dATP opposite the template 5′-neighbor dT is followed by extension, then the outcome would instead be a −1 deletion.

The single nucleotide insertion assays with the Sequence II 13-mer template:primer suggest that following insertion of dCTP opposite the AFB_1—N7-dG adduct, the Dpo4 polymerase can insert dATP opposite the template 5′-neighbor dT (Figure 1). In contrast, extension of the primer following insertion of dCTP opposite the AFB_1—β-FAPY adduct appears to be more difficult (Figure 2). In both the ternary complexes involving these adducts with the Sequence II template:primer and incoming dATP (Figures 4 and 7) either the guanine or the FAPY base conserves Watson—Crick hydrogen bonds with the 3′-primer terminus dC, potentially positioning the primer 3′-OH for a catalytic cycle. The incoming dATP forms Watson—Crick

hydrogen bonds with the template 5′-neighbor dT. One difference between the two structures is the distance between the α-phosphate of the incoming dATP and the 3′-OH group of the primer. This is 6.7 Å for the AFB$_1$—N7-dG adduct but increases to 6.9 Å for the AFB$_1$—β-FAPY adduct. Perhaps this can be attributed to the oxygen atom of the FAPY formamide group participating in a water-mediated hydrogen bond with Arg332 (Figure 8). Neither of these structures are likely to be catalytically efficient, due to the greater than 6 Å distances between the α-phosphates of the incoming dATPs and the 3′-OH groups of the primers. However, one could envision transient molecular motions bringing these atoms sufficiently close to allow phosphodiester bond formation. Both of these structures (Figures 4 and 7) are reminiscent of the "Type II" structure observed for ternary complexes of the Dpo4 polymerase with undamaged DNA.[47] In the Type II structure, the polymerase utilizes its expansive active site to accommodate two template nucleotides, and it inserts the dATP opposite the template 5′-neighbor nucleotide, rather than the damaged nucleotide. Remarkably, in these instances the active site of the polymerase accommodates the guanine or the FAPY base, the AFB$_1$ moiety, and the template 5′-neighbor dT. Thus, these could be considered to be "pseudo" Type II structures.

The similar ternary structures showing the misinsertion of incoming dTTP with the 5′- neighboring template dT, observed for both the AFB$_1$—N7-dG and the AFB$_1$—β-FAPY adducts (Figures 5 and 9) would lead to a T→A transversion at the 5′-neighbor base pair. However, single nucleotide insertion assays using the Sequence II 13-mer template:primer involving the AFB$_1$—N7-dG adduct show that correct insertion of dATP is strongly favored (Figure 1). A possible interpretation of the crystallographic data is that the Dpo4 polymerase can misinsert dTTP from the primed AFB$_1$—N7-dG:dC complex but cannot efficiently catalyze phosphodiester bond formation from this misinsertion complex. Similarly, single nucleotide insertion assays using the Sequence II template:primer involving the AFB$_1$—FAPY adduct (Figure 2) show that the Dpo4 polymerase is not efficient at extending nucleotides past the AFB$_1$—β-FAPY adduct. Again, it seems plausible that this polymerase does not efficiently catalyze phosphodiester bond formation from this misinsertion complex. In both cases, this may be due to the formation of hydrogen bonds between the N3 imino proton of the template T and the O^2 keto oxygen of the incoming dTTP, and between the O^4 keto oxygen of the template T and the N3 imino proton of the incoming dTTP. This pairing arrangement shifts the incoming dTTP toward the minor groove, relative to the position it would assume in a nascent A:T base pair.

Error-Prone Replication Past Other Bulky Aromatic Adducts. These structures of the Dpo4 polymerase in complex with AFB$_1$ adducts add to the structural database of Y-family polymerases interacting with bulky aromatic adducts, including aminofluorene and acetylaminofluorene,[68,72−74] and benzo[a]pyrene.[75] The Y-family polymerases probably exploit multiple mechanisms to bypass these bulky and conformationally complex lesions. For example, the interactions of bulky aromatic C8-dG aminofluorene vs acetylaminofluorene lesions differ depending upon whether the lesions are acetylated or nonacetylated. The nonacetylated lesions rotate about the glycosyl bond from the syn to the anti conformation in the primer—template complex,[68,72,73] whereas pol η interacts with the acetylated adducts without rotation into the anti conformation.[74] Crystallographic analysis of an N^6-dA benzo[a]pyrene adduct

complexed with the Dpo4 polymerase and an incoming nucleotide revealed two conformations, one intercalated 5′ to the template—primer terminus and the other in the major groove; it was proposed that the latter conformation might facilitate lesion bypass, suggesting that bypass requires flipping the intercalated lesion into the major groove.[75] Unlike these other bulky aromatic adducts AFB$_1$ remains intercalated at the active site and lesion bypass does not appear to involve reorientation of the lesion or extrusion into the major groove.

Summary. The Y-family *Sulfolobus solfataricus* P2 DNA polymerase IV (Dpo4) polymerase bypasses the AFB$_1$—N7-dG adduct, consistent with the low levels of G→T mutations observed for the AFB$_1$—N7-dG adduct in *E. coli*. However, the Dpo4 polymerase replicates past the AFB$_1$—β-FAPY adduct in an error-prone fashion. A series of binary (Dpo4—DNA) and ternary (Dpo4—DNA—dNTP) structures with site-specifically AFB$_1$—N7-dG and AFB$_1$—β-FAPY adducted templates suggest that differences resulting from differing orientations of the N7—C8 bond of the AFB$_1$—N7-dG adduct as compared to the N^5—C8 bond in the AFB$_1$—β-FAPY adduct, and resulting in differential accommodation of the planar AFB$_1$ moiety within the active site, may modulate AFB$_1$ lesion bypass by this polymerase.

■ EXPERIMENTAL PROCEDURES

Chemicals. The *Sulfolobus solfataricus* P2 DNA polymerase IV-(Dpo4) was expressed in *E. coli* and purified as described by Zang et al.[43] All dNTPs were obtained from Amersham Biosciences (Piscataway, NJ). Unmodified oligodeoxynucleotides were synthesized and purified by the Midland Certified Reagent Co. (Midland, TX), with analysis by MALDI mass spectrometry. The oligodeoxynucleotides 5′-d(TCATTGAATCCTTCCCCC)-3′,5′-d(GGGGGAAGGATTC)-3′ and 5′-d(GGGGGAAGGATT)-3′ were purchased from the Midland Certified Reagent Co. (Midland, TX) and purified by reverse-phase HPLC. Their concentrations were measured by UV absorbance at 260 nm.[76] Dimethyldioxirane was synthesized and assayed as described;[77−79] solutions were stored over anhydrous MgSO$_4$ at −20 °C and used within 1 week of preparation. AFB$_1$ was purchased from the Aldrich Chemical Co (Milwaukee, WI). AFB$_1$-exo-8,9-epoxide was prepared as described.[80] *Caution: AFB$_1$ is a potent liver toxin and is genotoxic, and it should be presumed that AFB$_1$-exo-8,9-epoxide is toxic and genotoxic. Crystalline aflatoxins are hazardous due to their electrostatic nature. AFB$_1$ can be destroyed by oxidation with NaOCl. Manipulations should be carried out in a well-ventilated hood with suitable containment procedures.*

Synthesis of Site-Specifically Modified Templates. The oligodeoxynucleotide 5′-d(TCATT$\underline{G}$AATCCTTCCCCC)-3′, containing the targeted N7-dG alkylation site (underlined), was annealed with 5′-d(ATTCAAT)-3′ in 100 mL of 100 mM sodium phosphate buffer (pH 6.5) to form a partially double-stranded scaffold. AFB$_1$-exo-8,9-epoxide (1 mg) was dissolved in 100 μL of anhydrous CH$_2$Cl$_2$ to produce a 3.2 mM solution. The epoxide was added in two 50 μL aliquots to the oligodeoxynucleotide solution at 5 °C, to create a 5:1 AFB$_1$-exo-8,9-epoxide:oligodeoxynucleotide molar ratio. The biphasic mixture was stirred at 5 °C for 15 min. The product 5′-d-(TCATT$\underline{X}$AATCCTTCCCCC)-3′ (X = AFB$_1$—N7-dG) was separated from 5′-d(TCATT$\underline{G}$AATCCTTCCCCC)-3′ and 5′-d(ATTCAAT)-3′ using HPLC (Gemini C-18 250 mm × 10 mm column, Phenomenex Inc., Torrance, CA) at a flow rate of 2 mL/min, with a linear 25 min gradient of 6% to 30% CH$_3$CN in 0.1 M ammonium formate (pH 8.0). The eluant was monitored by UV absorbance at 260 and 360 nm. The yield of 5′-d(TCATT$\underline{X}$AATCCTTCCCCC)-3′ (X = AFB$_1$—N7-dG) was 90%. The AFB$_1$—N7-dG-modified oligodeoxynucleotide was then used for crystallography, bypass studies, or as starting material for

producing the AFB$_1$−FAPY adduct. To produce the AFB$_1$−FAPY-modified template the 5′-d(TCATTXAATCCTTCCCCC)-3′ (X = AFB$_1$−N7-dG) oligodeoxynucleotide was suspended in 500 mL of 100 mM Na$_2$CO$_3$ at 37 °C (pH 10). The AFB$_1$−α-FAPY- and AFB$_1$−β-FAPY-modified DNA was separated by HPLC as described above and collected in a saturated Na$_2$HPO$_4$ solution. The AFB$_1$-α-FAPY-modified 5′-d(CTATXATTCA)-3′ oligodeoxynucleotide was desalted using a C-18 Sep-Pak cartridge (Waters Corp, Milford, MA) before annealing with its complement in a 1:1 molar ratio for subsequent crystallography or bypass experiments.

Single-Nucleotide Insertion Assays. The ^{32}P-labeled primer, was annealed to either unmodified or modified templates by heating a 1:1 molar ratios in 50 mM Tris-HCl buffer (pH 7.8) to 95 °C for 5 min and then cooling to room temperature. The unmodified and modified primers were extended in the presence of single dNTPs. Single nucleotide insertion studies were carried out at 37 °C. Each reaction was initiated by adding 2 μL of dNTP (final concentrations of 20, 50, 100 μM) to a preincubated template−primer−polymerase mixture [final concentrations of 50 mM Tris-HCl (pH 7.8), 50 mM NaCl, 5 mM MgCl$_2$, 1 mM DTT, 50 μg/mL BSA, 100 nM DNA, and 100 nM Dpo4] at 37 °C, yielding a total reaction volume of 10 μL. The reaction mixtures for unmodified template:primers were incubated over a time period of 5 min and those of modified template:primers for 60 min. Each reaction was quenched with 50 μL of 20 mM Na$_2$EDTA (pH 9.0) in 95% formamide (v/v) containing xylenecyanol and bromophenol blue dyes and heated at 95 °C for 10 min. Aliquots (6 μL) were separated by electrophoresis on a denaturing gel containing 8.0 M urea and 16% acrylamide (w/v) (from a 19:1 acrylamide−bisacrylamide solution, AccuGel, National Diagnostics, Atlanta, GA) with 80 mM Tris borate buffer (pH 7.8) containing 1 mM Na$_2$EDTA. The gel was exposed to a PhosphorImager screen (Imaging Screen K, Bio-Rad) overnight. The bands were visualized with a PhosphorImaging system (Bio-Rad, Molecular Imager FX) using the manufacturer's software Quantity One, version 4.3.0.

Full-Length Polymerase Extension Assays. The primers were extended in the presence of all four dNTPs. Each reaction was initiated by adding 2 μL of all four dNTPs (final concentrations of 20, 50, 100 μM) to a preincubated template−primer−polymerase reaction mixture [final concentrations of 50 mM Tris-HCl (pH 7.8), 50 mM NaCl, 5 mM MgCl$_2$, 1 mM DTT, 50 μg/mL BSA, 100 nM DNA duplex, and 100 nM Dpo4] at 37 °C, yielding a total reaction volume of 10 μL. The reaction mixtures for unmodified template:primers were incubated over a time period of 5 min and that of modified template:primers for 60 min. The reactions were quenched and analyzed by gel electrophoresis as described above.

Crystallization of Dpo4−DNA Complexes. The lengths of the primers and templates were similar to those used by Ling et al.[47] The 18-mer template containing either the AFB$_1$−N7-dG or AFB$_1$−β-FAPY adduct was annealed with the Sequence I 12-mer or Sequence II 13-mer primer at a 1:1 molar ratio in 0.1 M NaCl, 10 mM NaH$_2$PO$_4$, and 50 μM Na$_2$EDTA (pH 7.2). The duplexes were eluted from DNA grade hydroxyapatite (Bio-Rad Laboratories, Richmond, CA) with a gradient from 10 to 200 mM NaH$_2$PO$_4$ in 10 mM NaH$_2$PO$_4$, 0.1 M NaCl, and 50 μM EDTA (pH 7.0). Duplexes were desalted with Sephadex G-25. The Dpo4 polymerase was concentrated to 50−70 mg/mL using a spin concentrator with a 10^4 M$_r$ Amicon cutoff filter (Millipore, Inc., Billerica, MA) in 50 mM Tris-HCl (pH 7.4 at 25 °C) buffer containing 100 mM NaCl, 5 mM β-mercaptoethanol, and 50% glycerol (v/v). For both the AFB$_1$−N7-dG and AFB$_1$−β-FAPY adducts, crystallization trials were conducted for binary (template:primer·polymerase) and ternary (template:primer·polymerase·dNTP) complexes in the presence of Ca^{2+} and in the presence of each of the four possible dNTPs. The Dpo4 polymerase was combined with DNA (1:1.2 molar ratio) and then placed on ice for 1 h prior to incubation with 1 mM dNTP and 5 mM

CaCl$_2$. The concentration range of 7−15 mg/mL of the polymerase was used to find the optimum concentration for growing crystals that diffracted well. Crystals were grown using the sitting drop vapor diffusion method by mixing 1 μL of complex with 1 μL of a solution containing 50 mM Tris-HCl (pH 7.4 at 25 °C) buffer, 12−20% polyethylene glycol 3350 (w/v), 100 mM Ca(OAc)$_2$, and 2.5% glycerol (v/v). Crystals were soaked in mother liquor containing an additional 25% polyethylene glycol 3350 (w/v) and 15% ethylene glycol (v/v) and flash-frozen in a stream of liquid nitrogen.

X-ray Diffraction Data Collection and Processing. All diffraction data sets for binary and ternary complexes were collected at 110 K using a synchrotron radiation wavelength around 1.00 Å on the 22-ID (SER-CAT) or 21-ID (LS-CAT) beamlines at the Advanced Photon Source (Argonne, IL). Indexing and scaling were performed using HKL2000.[81] The data were processed using CCP4 package programs, and the truncate procedure was performed with TRUNCATE.[82]

Structure Determination and Refinement. A refined structure (PDB entry 2BQU) downloaded from Protein Data Bank was used as a starting model by modifying the template and primer and inserting the AFB$_1$−N7-dG or the AFB$_1$−β-FAPY adduct. The cross-rotation and cross-translation functions were used to align the model with the experimental data. In each instance, several rounds of rigid body refinement of the diffraction data, with gradually increasing resolution, optimized the initial positions of the models. The model was refined further using CNS Solve (version 1.1),[44] including simulated annealing, gradient minimization, individual occupancy, and refinement of individual isotropic temperature factors. Manual model building was performed using TURBO-FRODO.[83,84] A total of 5−10% of the reflections were excluded from the refinement to calculate the cross-validation residual R$_{free}$. Water oxygen atoms were added into positive regions (more than 3.0 standard deviations) of F$_o$ − F$_c$ Fourier difference electron density during the manual model rebuilding steps. The crystallographic figures were prepared using PyMOL.[85]

Data Deposition. Complete structure factor and final coordinates were deposited in the Protein Data Bank (www.rcsb.org): PDB ID codes for the ternary complexes of the AFB$_1$−N7-dG adduct with dCTP, 3PW7; with dATP, 3PW4; with dTTP, 3PW5; for the binary complex of the AFB$_1$−β-FAPY, 3PVX; for the ternary complex of the AFB$_1$−β-FAPY adduct with dATP, 3PW0; with dTTP, 3PW2.

■ ASSOCIATED CONTENT

S **Supporting Information.** Tables S1, crystal data and refinement parameters for the ternary complexes with the AFB$_1$−N7-dG adduct, and S2, crystal data and refinement parameters for the binary and ternary complexes with the AFB$_1$−β-FAPY adduct. This material is available free charge via the Internet at http://pubs.acs.org.

■ AUTHOR INFORMATION

Corresponding Author
michael.p.stone@vanderbilt.edu

Present Address
§Northeastern Collaborative Access Team and Department of Chemistry and Chemical Biology, Cornell University, Building 436E, Argonne National Laboratory, Argonne, IL 60439.

■ ACKNOWLEDGMENT

■ REFERENCES

(1) Busby, W. F., Jr.; Wogan, G. N. In *Chemical Carcinogens*, 2nd ed.; Searle, C. E., Ed.; American Chemical Society: Washington, D.C., 1984, pp 945−1136.

(2) Smela, M. E.; Currier, S. S.; Bailey, E. A.; Essigmann, J. M. *Carcinogenesis* **2001**, *22*, 535−545.

(3) Bennett, J. W.; Klich, M. *Clin. Microbiol. Rev.* **2003**, *16*, 497−516.

(4) Kensler, T. W.; Roebuck, B. D.; Wogan, G. N.; Groopman, J. D. *Toxicol. Sci.* **2011**, *120* (Suppl 1), S28−48.

(5) McCann, J.; Spingarn, N. E.; Koburi, J.; Ames, B. N. *Proc. Natl. Acad. Sci. U.S.A.* **1975**, *72*, 979−983.

(6) Foster, P. L.; Eisenstadt, E.; Miller, J. H. *Proc. Natl. Acad. Sci. U.S.A.* **1983**, *80*, 2695−2698.

(7) Foster, P. L.; Groopman, J. D.; Eisenstadt, E. *J. Bacteriol.* **1988**, *170*, 3415−3420.

(8) Bailey, G. S.; Williams, D. E.; Wilcox, J. S.; Loveland, P. M.; Coulombe, R. A.; Hendricks, J. D. *Carcinogenesis* **1988**, *9*, 1919−1926.

(9) Bailey, G. S.; Loveland, P. M.; Pereira, C.; Pierce, D.; Hendricks, J. D.; Groopman, J. D. *Mutat. Res.* **1994**, *313*, 25−38.

(10) McMahon, G.; Davis, E. F.; Huber, L. J.; Kim, Y.; Wogan, G. N. *Proc. Natl. Acad. Sci. U.S.A.* **1990**, *87*, 1104−1108.

(11) Soman, N. R.; Wogan, G. N. *Proc. Natl. Acad. Sci. U.S.A.* **1993**, *90*, 2045−2049.

(12) Yang, M.; Zhou, H.; Kong, R. Y.; Fong, W. F.; Ren, L. Q.; Liao, X. H.; Wang, Y.; Zhuang, W.; Yang, S. *Mutat. Res.* **1997**, *381*, 25−29.

(13) Groopman, J. D.; Kensler, T. W. *Toxicol. Appl. Pharmacol.* **2005**, *206*, 131−137.

(14) Bressac, B.; Kew, M.; Wands, J.; Ozturk, M. *Nature* **1991**, *350*, 429−431.

(15) Hsu, I. C.; Metcalf, R. A.; Sun, T.; Welsh, J. A.; Wang, N. J.; Harris, C. C. *Nature* **1991**, *350*, 427−428.

(16) Greenblatt, M. S.; Bennett, W. P.; Hollstein, M.; Harris, C. C. *Cancer Res.* **1994**, *54*, 4855−4878.

(17) Shen, H. M.; Ong, C. N. *Mutat. Res.* **1996**, *366*, 23−44.

(18) Soini, Y.; Chia, S. C.; Bennett, W. P.; Groopman, J. D.; Wang, J. S.; DeBenedetti, V. M.; Cawley, H.; Welsh, J. A.; Hansen, C.; Bergasa, N. V.; Jones, E. A.; DiBisceglie, A. M.; Trivers, G. E.; Sandoval, C. A.; Calderon, I. E.; Munoz Espinosa, L. E.; Harris, C. C. *Carcinogenesis* **1996**, *17*, 1007−1012.

(19) Lunn, R. M.; Zhang, Y. J.; Wang, L. Y.; Chen, C. J.; Lee, P. H.; Lee, C. S.; Tsai, W. Y.; Santella, R. M. *Cancer Res.* **1997**, *57*, 3471−3477.

(20) Mace, K.; Aguilar, F.; Wang, J. S.; Vautravers, P.; Gomez-Lechon, M.; Gonzalez, F. J.; Groopman, J.; Harris, C. C.; Pfeifer, A. M. *Carcinogenesis* **1997**, *18*, 1291−1297.

(21) Shimada, T.; Guengerich, F. P. *Proc. Natl. Acad. Sci. U.S.A.* **1989**, *86*, 462−465.

(22) Raney, K. D.; Shimada, T.; Kim, D. H.; Groopman, J. D.; Harris, T. M.; Guengerich, F. P. *Chem. Res. Toxicol.* **1992**, *5*, 202−210.

(23) Ueng, Y. F.; Shimada, T.; Yamazaki, H.; Guengerich, F. P. *Chem. Res. Toxicol.* **1995**, *8*, 218−225.

(24) Gallagher, E. P.; Kunze, K. L.; Stapleton, P. L.; Eaton, D. L. *Toxicol. Appl. Pharmacol.* **1996**, *141*, 595−606.

(25) Johnson, W. W.; Harris, T. M.; Guengerich, F. P. *J. Am. Chem. Soc.* **1996**, *118*, 8213−8220.

(26) Essigmann, J. M.; Croy, R. G.; Nadzan, A. M.; Busby, W. F., Jr.; Reinhold, V. N.; Buchi, G.; Wogan, G. N. *Proc. Natl. Acad. Sci. U.S.A.* **1977**, *74*, 1870−1874.

(27) Gopalakrishnan, S.; Byrd, S.; Stone, M. P.; Harris, T. M. *Biochemistry* **1989**, *28*, 726−734.

(28) Iyer, R. S.; Coles, B. F.; Raney, K. D.; Thier, R.; Guengerich, F. P.; Harris, T. M. *J. Am. Chem. Soc.* **1994**, *116*, 1603−1609.

(29) Hertzog, P. J.; Smith, J. R. L.; Garner, R. C. *Carcinogenesis* **1982**, *3*, 723−725.

(30) Brown, K. L.; Deng, J. Z.; Iyer, R. S.; Iyer, L. G.; Voehler, M. W.; Stone, M. P.; Harris, C. M.; Harris, T. M. *J. Am. Chem. Soc.* **2006**, *128*, 15188−15199.

(31) Smela, M. E.; Hamm, M. L.; Henderson, P. T.; Harris, C. M.; Harris, T. M.; Essigmann, J. M. *Proc. Natl. Acad. Sci. U.S.A.* **2002**, *99*, 6655−6660.

(32) Bailey, E. A.; Iyer, R. S.; Stone, M. P.; Harris, T. M.; Essigmann, J. M. *Proc. Natl. Acad. Sci. U.S.A.* **1996**, *93*, 1535−1539.

(33) Hertzog, P. J.; Lindsay Smith, J. R.; Garner, R. C. *Carcinogenesis* **1980**, *1*, 787−793.

(34) Croy, R. G.; Wogan, G. N. *Cancer Res.* **1981**, *41*, 197−203.

(35) Groopman, J. D.; Croy, R. G.; Wogan, G. N. *Proc. Natl. Acad. Sci. U.S.A.* **1981**, *78*, 5445−5449.

(36) Mao, H.; Deng, Z.; Wang, F.; Harris, T. M.; Stone, M. P. *Biochemistry* **1998**, *37*, 4374−4387.

(37) Giri, I.; Stone, M. P. *Biopolymers* **2002**, *65*, 190−201.

(38) Gopalakrishnan, S.; Harris, T. M.; Stone, M. P. *Biochemistry* **1990**, *29*, 10438−10448.

(39) Johnston, D. S.; Stone, M. P. *Biochemistry* **1995**, *34*, 14037−14050.

(40) Jones, W. R.; Johnston, D. S.; Stone, M. P. *Chem. Res. Toxicol.* **1998**, *11*, 873−881.

(41) Giri, I.; Jenkins, M. D.; Schnetz-Boutaud, N. C.; Stone, M. P. *Chem. Res. Toxicol.* **2002**, *15*, 638−647.

(42) Brown, K. L.; Voehler, M. W.; Magee, S. M.; Harris, C. M.; Harris, T. M.; Stone, M. P. *J. Am. Chem. Soc.* **2009**, *131*, 16096−16107.

(43) Zang, H.; Goodenough, A. K.; Choi, J. Y.; Irimia, A.; Louka-chevitch, L. V.; Kozekov, I. D.; Angel, K. C.; Rizzo, C. J.; Egli, M.; Guengerich, F. P. *J. Biol. Chem.* **2005**, *280*, 29750−29764.

(44) Brunger, A. T.; Adams, P. D.; Clore, G. M.; DeLano, W. L.; Gros, P.; Grosse-Kunstleve, R. W.; Jiang, J. S.; Kuszewski, J.; Nilges, M.; Pannu, N. S.; Read, R. J.; Rice, L. M.; Simonson, T.; Warren, G. L. *Acta Crystallogr., Sect. D: Biol. Crystallogr.* **1998**, *54*, 905−921.

(45) Vagin, A.; Teplyakov, A. *J. Appl. Crystallogr.* **1997**, *30*, 1022−1025.

(46) Vagin, A.; Teplyakov, A. *Acta Crystallogr. D: Biol. Crystallogr.* **2010**, *66*, 22−25.

(47) Ling, H.; Boudsocq, F.; Woodgate, R.; Yang, W. *Cell* **2001**, *107*, 91−102.

(48) Silvian, L. F.; Toth, E. A.; Pham, P.; Goodman, M. F.; Ellenberger, T. *Nat. Struct. Biol.* **2001**, *8*, 984−989.

(49) Goodman, M. F. *Annu. Rev. Biochem.* **2002**, *71*, 17−50.

(50) Alt, A.; Lammens, K.; Chiocchini, C.; Lammens, A.; Pieck, J. C.; Kuch, D.; Hopfner, K. P.; Carell, T. *Science* **2007**, *318*, 967−970.

(51) Reissner, T.; Schneider, S.; Schorr, S.; Carell, T. *Angew. Chem., Int. Ed.* **2010**, *49*, 3077−3080.

(52) Silverstein, T. D.; Johnson, R. E.; Jain, R.; Prakash, L.; Prakash, S.; Aggarwal, A. K. *Nature* **2010**, *465*, 1039−1043.

(53) Rechkoblit, O.; Malinina, L.; Cheng, Y.; Kuryavyi, V.; Broyde, S.; Geacintov, N. E.; Patel, D. J. *PLoS Biol.* **2006**, *4*, e11.

(54) Johnson, R. E.; Prakash, S.; Prakash, L. *Proc. Natl. Acad. Sci. U.S.A.* **2000**, *97*, 3838−3843.

(55) Zhang, Y.; Yuan, F.; Wu, X.; Rechkoblit, O.; Taylor, J. S.; Geacintov, N. E.; Wang, Z. *Nucleic Acids Res.* **2000**, *28*, 4717−4724.

(56) Ohashi, E.; Bebenek, K.; Matsuda, T.; Feaver, W. J.; Gerlach, V. L.; Friedberg, E. C.; Ohmori, H.; Kunkel, T. A. *J. Biol. Chem.* **2000**, *275*, 39678−39684.

(57) Boudsocq, F.; Iwai, S.; Hanaoka, F.; Woodgate, R. *Nucleic Acids Res.* **2001**, *29*, 4607−4616.

12567

dx.doi.org/10.1021/ja2015668 |*J. Am. Chem. Soc.* 2011, 133, 12556−12568

(58) Gerlach, V. L.; Feaver, W. J.; Fischhaber, P. L.; Friedberg, E. C. *J. Biol. Chem.* **2001**, *276*, 92–98.

(59) Johnson, R. E.; Prakash, S.; Prakash, L. *Science* **1999**, *283*, 1001–1004.

(60) Ohashi, E.; Ogi, T.; Kusumoto, R.; Iwai, S.; Masutani, C.; Hanaoka, F.; Ohmori, H. *Genes Dev.* **2000**, *14*, 1589–1594.

(61) Haracska, L.; Yu, S. L.; Johnson, R. E.; Prakash, L.; Prakash, S. *Nat. Genet.* **2000**, *25*, 458–461.

(62) Johnson, R. E.; Washington, M. T.; Haracska, L.; Prakash, S.; Prakash, L. *Nature* **2000**, *406*, 1015–1019.

(63) Frank, E. G.; Sayer, J. M.; Kroth, H.; Ohashi, E.; Ohmori, H.; Jerina, D. M.; Woodgate, R. *Nucleic Acids Res.* **2002**, *30*, 5284–5292.

(64) Rechkoblit, O.; Zhang, Y.; Guo, D.; Wang, Z.; Amin, S.; Krzeminsky, J.; Louneva, N.; Geacintov, N. E. *J. Biol. Chem.* **2002**, *277*, 30488–30494.

(65) Huang, X.; Kolbanovskiy, A.; Wu, X.; Zhang, Y.; Wang, Z.; Zhuang, P.; Amin, S.; Geacintov, N. E. *Biochemistry* **2003**, *42*, 2456–2266.

(66) Washington, M. T.; Minko, I. G.; Johnson, R. E.; Haracska, L.; Harris, T. M.; Lloyd, R. S.; Prakash, S.; Prakash, L. *Mol. Cell. Biol.* **2004**, *24*, 6900–6906.

(67) Washington, M. T.; Minko, I. G.; Johnson, R. E.; Wolfle, W. T.; Harris, T. M.; Lloyd, R. S.; Prakash, S.; Prakash, L. *Mol. Cell. Biol.* **2004**, *24*, 5687–5693.

(68) Rechkoblit, O.; Kolbanovskiy, A.; Malinina, L.; Geacintov, N. E.; Broyde, S.; Patel, D. J. *Nat. Struct. Mol. Biol.* **2010**, *17*, 379–388.

(69) Wong, J. H.; Brown, J. A.; Suo, Z.; Blum, P.; Nohmi, T.; Ling, H. *EMBO J.* **2010**, *29*, 2059–2069.

(70) Nair, D. T.; Johnson, R. E.; Prakash, S.; Prakash, L.; Aggarwal, A. K. *Nature* **2004**, *430*, 377–380.

(71) Wong, J. H.; Fiala, K. A.; Suo, Z.; Ling, H. *J. Mol. Biol.* **2008**, *379*, 317–330.

(72) Dutta, S.; Li, Y.; Johnson, D.; Dzantiev, L.; Richardson, C. C.; Romano, L. J.; Ellenberger, T. *Proc. Natl. Acad. Sci. U.S.A.* **2004**, *101*, 16186–16191.

(73) Hsu, G. W.; Kiefer, J. R.; Burnouf, D.; Becherel, O. J.; Fuchs, R. P.; Beese, L. S. *J. Biol. Chem.* **2004**, *279*, 50280–50285.

(74) Schorr, S.; Schneider, S.; Lammens, K.; Hopfner, K. P.; Carell, T. *Proc. Natl. Acad. Sci. U.S.A.* **2010**, *107*, 20720–20725.

(75) Ling, H.; Sayer, J. M.; Plosky, B. S.; Yagi, H.; Boudsocq, F.; Woodgate, R.; Jerina, D. M.; Yang, W. *Proc. Natl. Acad. Sci. U.S.A.* **2004**, *101*, 2265–2269.

(76) Cavaluzzi, M. J.; Borer, P. N. *Nucleic Acids Res.* **2004**, *32*, e13.

(77) Murray, R. W.; Jeyaraman, R. *J. Org. Chem.* **1985**, *50*, 2847–2853.

(78) Adam, W.; Chan, Y. Y.; Cremer, D.; Gauss, J.; Scheutzow, D.; Schindler, M. *J. Org. Chem.* **1987**, *52*, 2800–2803.

(79) Adam, W.; Bialas, J.; Hadjiarapoglou, L. *Chem. Ber.* **1991**, *124*, 2377–2377.

(80) Baertschi, S. W.; Raney, K. D.; Stone, M. P.; Harris, T. M. *J. Am. Chem. Soc.* **1988**, *110*, 7929–7931.

(81) Otwinowski, Z.; Minor, W. *Acta Crystallogr., Sect. A: Found. Crystallogr.* **1997**, *276*, 307–326.

(82) French, S.; Wilson, K. *Acta Crystallogr., Sect. A: Found. Crystallogr.* **1978**, *34*, 517–525.

(83) Vellieux, F. M. D.; Dijkstra, B. W. *J. Appl. Crystallogr.* **1997**, *30*, 396–399.

(84) Cambillau, C.; Roussel, A. *TURBO FRODO Version OpenGL.1*; Université Aix-Marseille II, Marseille, France, 1997.

(85) DeLano, W. L. *PyMOL*; DeLano Scientific LLC, Palo Alto, CA, 2008.